

1 **Local Magnitude Discrepancies for Near-Event Receivers; Implications for the UK Traffic**  
2 **Light Scheme**

3 **Antony Butcher<sup>1\*</sup>, Richard Lockett<sup>2</sup>, James P Verdon<sup>1</sup>, J-Michael Kendall<sup>1</sup>, Brian Baptie<sup>2</sup>**  
4 **& James Wookey<sup>1</sup>**

5 <sup>1</sup> School of Earth Sciences, University of Bristol, Wills Memorial Building, Queen's Road, Bristol BS8 1RJ, UK

6 <sup>2</sup> British Geological Survey, Earthquake Seismology, Edinburgh, EH14 4AP, United Kingdom

7 \*Tel: +44 7813174568; Email: [antony.butcher@bristol.ac.uk](mailto:antony.butcher@bristol.ac.uk)

9 **Abstract**

10 Local seismic magnitudes provide a practical scale for quick implementation of regulation  
11 designed to manage the risk of induced seismicity, such as Traffic Light Schemes. We  
12 demonstrate that significant magnitude discrepancies occur when seismic events are recorded  
13 on nearby stations (<5km), which can be a unit higher values than those observed on more  
14 distant stations. This is due to the influence of sedimentary layers, as these shallow layers are  
15 generally lower in velocity and more attenuating than the underlying crystalline basement rocks,  
16 and require a change in the attenuation term of the  $M_L$  scale. This has a significant impact on the  
17 UK's hydraulic fracturing Traffic Light Scheme whose 'red' light is set at  $M_L = 0.5$ . As the nominal  
18 detectability of the UK network is  $M_L = 2$ , this scheme will entail the deployment of monitoring  
19 stations in close proximity to well sites. Using data collected from mining events near New  
20 Ollerton, Nottinghamshire, we illustrate the effects proximity has on travel path velocities and  
21 attenuation, then perform a damped least squares inversion to determine appropriate constants  
22 within the  $M_L$  scale. We show that the attenuation term needs to increase from 0.00183 to 0.0514,  
23 and demonstrate that this higher value is representative of a raypath within a slower, more  
24 attenuating sedimentary layer compared to the continental crust. We therefore recommend that  
25 the magnitude scale  $M_L = \log(A) + 1.17\log(r) + 0.0514r - 3.0$  should be used when local  
26 monitoring networks are within 5km of the event epicentres.

27 **Keywords:** Earthquake monitoring, Induced seismicity, Seismic attenuation

## 28 1. Introduction

29 Any subsurface activity that alters the state of stress in the ground is capable of triggering seismic  
30 activity on pre-existing faults. In the United Kingdom (UK), coal mining has long been the  
31 dominant cause of these anthropogenic events (Wilson et al. 2015). However, with the coal  
32 industry in decline, concerns about induced seismicity have switched to the nascent shale gas  
33 industry.

34 In response to these concerns, the UK's Oil and Gas Authority has imposed a Traffic Light  
35 Scheme (TLS) to manage induced seismicity, with an "amber" warning set at a magnitude of  $M_L$   
36 = 0.0, and a "red" light at  $M_L = 0.5$ , where injection must cease followed by a 24hr monitoring  
37 period (Department of Energy and Climate Change 2015). A local magnitude scale is used, as  
38 opposed to other scales such as the moment magnitude, as the measurement is less  
39 complicated: the local magnitude scale is empirical, directly relating the measured maximum  
40 displacement amplitude (typically associated with the S-wave arrival) and hypocentral distance  
41 to  $M_L$ . For such a scheme to maintain the confidence of both the industry, the regulators, and the  
42 general public, the local magnitude scale used to quantify event magnitudes must be robust and  
43 well constrained.

44 The existing UK local magnitude scale (Ottemöller & Sargeant 2013) was calibrated using larger  
45 events, most of which were recorded at considerable distance (>50km) from their epicentres. In  
46 contrast, the TLS will be administered with local networks within 5km of the epicentres of any  
47 events that may occur. In this paper we seek to highlight issues with the Local Magnitude ( $M_L$ )  
48 scale when used on shallow events located in close proximity to the receivers.

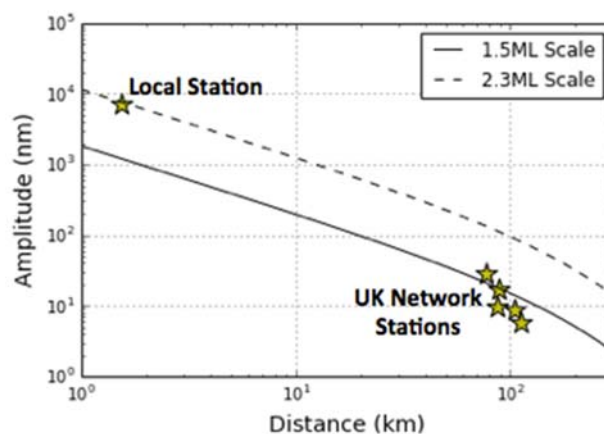
49 In April 2011, hydraulic fracturing operations at the Preese Hall well, near Blackpool UK, caused  
50 an  $M_L$  2.3 earthquake (Clarke et al. 2014). This event was felt by local people causing  
51 considerable public concern, despite its relatively small magnitude. In response the British  
52 Geological Survey (BGS) installed temporary seismic stations close to the epicentre and  
53 recorded several subsequent, smaller events during further hydraulic fracturing stages.

54 As the first recorded instance of seismicity induced by hydraulic fracturing in the UK, these events  
 55 have been the subject of much interest (e.g. O'Toole et al. 2013; Westaway 2016). One aspect  
 56 of the data that was immediately apparent was the discrepancy in local magnitude. Ground  
 57 motions measured using a local monitoring station located at hypocentral distances of 1.5km  
 58 differed significantly in comparison to those calculated using the national UK seismic monitoring  
 59 network, the nearest station of which was at a distance of approximately 80km.

60 Based on the existing local magnitude scale, the largest event recorded by both distant and local  
 61 stations had a magnitude of  $M_L = 1.5$  calculated on the national network, but  $M_L = 2.3$  on a local  
 62 station located at an epicentral distance of 1.5km (Figure 1). Because of this discrepancy,  
 63 magnitudes of events observed on only the Preese Hall network were assigned though scaling  
 64 relative to a 'master' event using the equation

$$65 \quad M_{DetectEvent} = M_{MasterEvent} - \log \left( \frac{A_{DetectEvent}}{A_{MasterEvent}} \right), \quad (1)$$

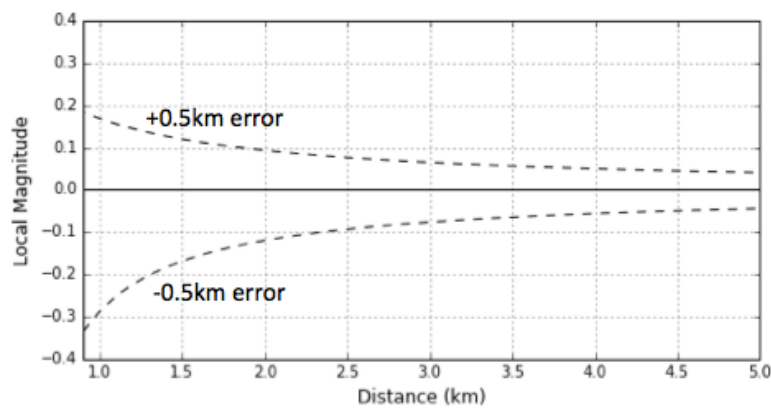
66 where A is the maximum amplitude measured on the waveform, and M is the magnitude of the  
 67 master or detected event (Eisner et al. 2011).



68 Figure 1: Measured ground displacements for the largest event at Preese Hall to be recorded by both  
 69 local and distant stations (yellow stars). The expected displacement for  $M_L = 1.4$  and  $M_L = 2.3$  events are  
 70 shown by the solid and dashed lines, respectively. These measurements show the discrepancies in  
 71 ground motion between a locally installed seismic station and the more distant UK seismic network.  
 72

73 The BGS seismic catalogue shows several other examples of magnitude discrepancies for

74 events in close proximity to receivers, and several studies have also identified either  
 75 overestimation in magnitudes or larger than predicted amplitudes at close distances in other  
 76 settings (Atkinson et al. 2014; Scognamiglio et al. 2012). A common explanation for these  
 77 discrepancies is that nearby stations may be more impacted by event location errors. However,  
 78 in Figure 2 we show the impact of a 0.5km location error: while nearby stations are more  
 79 impacted, the resulting magnitude error is insufficient to account for the discrepancies observed  
 80 at Preese Hall. Moreover, if event location errors, or local site effects, were causing magnitude  
 81 errors, we would expect these discrepancies to be random in nature, leading to both under- and  
 82 overestimates of event magnitudes. Instead, we tend to see only overestimation of magnitudes  
 83 at close distances: a systematic error implying a methodological issue with the use of local  
 84 magnitude scales.



85  
 86 Figure 2: Impact of a introducing a positional error of 0.5km on calculated magnitudes. At a distance of  
 87 1.5km, comparable to Preese Hall, the maximum magnitude discrepancy is no more than 0.2 units.

88 **2. Local Magnitude ( $M_L$ )**

89 Ottemöller and Sargeant (2013) developed the most recent  $M_L$  scale for the United Kingdom,  
 90 replacing the original Hutton and Boore (1987) scale which was derived for Southern California.  
 91 The inversion of 1482 observations from 85 earthquakes on 50 stations, anchored to a reference  
 92 distance of 100km led to the following local magnitude scale

93 
$$M_L = \log(A) + 0.95\log(r) + 0.00183r - 1.76 , (2)$$

94 where  $A$  is horizontal-component ground displacement amplitude filtered with Wood-Anderson  
95 response in nanometers and  $r$  is the hypocentral distance in km. As observations were taken  
96 from earthquakes recorded on the UK network, the dataset used by Ottemöller and Sargeant  
97 (2013) is dominated by events with magnitudes larger than  $M_L = 2.0$ , with epicentral distances  $>$   
98 50km. As a result the current UK  $M_L$  scale has not been well calibrated for small-magnitude, near-  
99 receiver events, such as those recorded at Preese Hall, or potentially at future shale gas  
100 extraction sites.

101 The Richter equation for  $M_L$  is defined as□

102 
$$M_L = \log(A_{WA}) - \log(A_0) + C , (3)$$

103 where  $A_{WA}$  is zero-to-peak amplitude measured on a standard horizontal Wood-Anderson  
104 seismograph,  $-\log(A_0)$  is the displacement correction term, and  $C$  is a correction term for  
105 individual stations. The displacement correction term accounts for geometrical spreading,  
106 attenuation, and calibrates the scale to Richter's original definition, while  $C$  is a constant used to  
107 correct site-effects at each station. In this equation, the displacement amplitude is given in mm,  
108 and gain corrected to a Wood-Anderson seismograph. To remove this requirement, the UK  $M_L$   
109 scale applies the gain correction

110 
$$\log(A_{WA}) = \log(A) + \log\left(\frac{2080}{10^6}\right). (4)$$

111 For a local earthquake, the S-wave amplitude  $A$  can be expressed as a function of hypocentral  
112 distance  $r$  by

113 
$$A(r) = A_0 r^{-\beta} e^{\frac{-\pi f r}{vQ}} , (5)$$

114 where  $A_0$  is the initial amplitude,  $\beta$  is the geometrical spreading,  $f$  is the frequency,  $v$  the path  
115 averaged S-wave velocity and  $Q$  the quality factor, which is inversely proportional to the anelastic  
116 attenuation. Havskov & Ottemoller (2010) show that by taking the logarithm of (5) produces

117 
$$\log(A(r)) = \log(r) - 0.43 \frac{\pi f r}{v Q} + \log(A_0) . (6)$$

118 If  $f$ ,  $v$  and  $Q$  are assumed to be constant, the displacement correction term can be expressed in  
119 the form

120 
$$-\log(A_0) = a \log(r) + br + c , (7)$$

121 where  $a$ ,  $b$  and  $c$  are constants representing geometrical spreading, attenuation and the base  
122 level respectively. Two different anchor points are commonly used to link the  $M_L$  scale to Richter's  
123 definition. Originally a magnitude 3.0 earthquake was defined as a 1mm displacement at 100km,  
124 and more recently a 10mm displacement at 17km has been used to adjust the scale to other  
125 regions with significantly different attenuation (Hutton & Boore 1987). Anchoring the  
126 displacement correction term to 17km results in the equation

127 
$$-\log(A_0) = a \log(r/17) + b(r - 17) + 2 . (8)$$

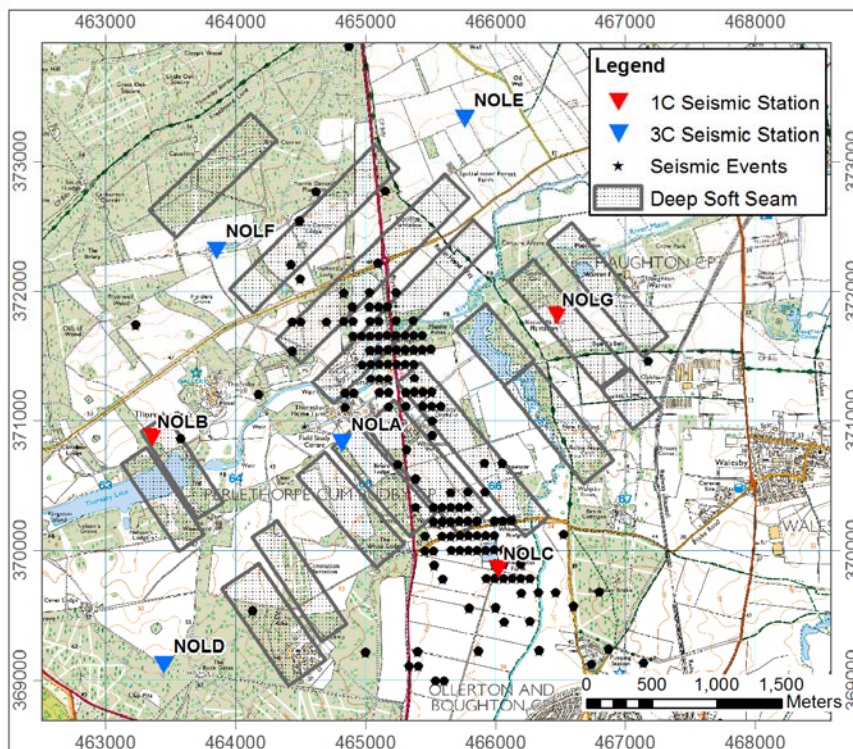
128 As the geometrical spreading does not vary significantly from 1, the greatest impact on the  $M_L$   
129 scale will be caused by changes to the attenuation term  $b$ . From equations (6) and (7), this term  
130 can be represented by the equation

131 
$$b \approx 0.43 \frac{\pi f}{v Q} . (9)$$

132 When considering shallow, nearby events we would expect a greater portion of the raypath to be  
133 through shallow sediments, as opposed to the more distant events used to calibrate the UK's  
134 present  $M_L$  scale, which will have travelled predominantly through the deeper crust. We would  
135 therefore anticipate that both  $Q$  and  $v$  would be lower. Furthermore, because the path distance  
136 will be smaller, the frequency content,  $f$ , would likely be higher. These effects will have the  
137 combined effect of significantly increasing the attenuation constant  $b$ , which will have different  
138 impacts on the displacement equation (8) depending on the distance. At distances less than the  
139 anchor point, an increase in  $b$  will decrease the actual magnitude of the event while at greater  
140 distances the magnitude will be increased.

141 **3. Data**

142 To examine the impact that the proximity of receivers to seismic events has on  $M_L$  estimations,  
143 we use a series of seismic events recorded to the north of New Ollerton, Nottinghamshire, UK.  
144 The area has a history of seismic activity relating to coal mining (Bishop et al. 1993), and the  
145 locations and characteristics are consistent with coal seams worked by Thoresby Colliery,  
146 located approximately 800-900m below the surface. The seams below this area are the Parkgate  
147 and Deep Soft, and borehole records show that they are overlain by strata of sandstone,  
148 limestones and marls (IMC Group Consulting Limited 2003). Deep Soft is the most recently  
149 operational seam, and was worked from 2010 until the closure of the colliery in July 2015. The  
150 coal was extracted using the longwall mining method, where the roof is supported while a cutting  
151 machine is pulled along the width of the coal face. As the machine moves forward, the supports  
152 are advanced and the roof behind the supports is allowed to fall into the void left by the coal.



153  
154 Figure 3: Location of New Ollerton Network (inverted triangles), recorded seismic events (black dots) and  
155 coal seam panels (grey rectangles).



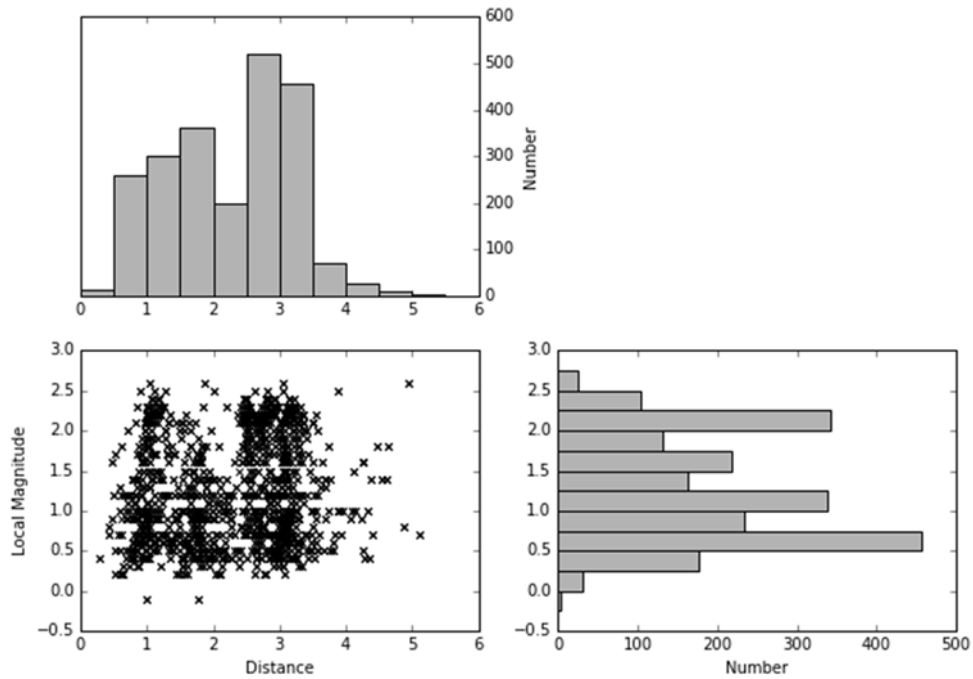
156 Between 5th February 2014 and 30th October 2014 a temporary network (here called NOL) was  
 157 deployed by the British Geological Survey, which comprised of four 3-component Guralp 3ESP  
 158 broadband instruments (NOLA, NOLD, NOLE and NOLF) and three vertical component S13J  
 159 instruments (NOLB, NOLC and NOLG) with an aperture of about 5km (Figure 3). During the  
 160 deployment over 300 events were identified, which were clustered in two distinct regions, and fell  
 161 within a source-receiver distance range of between 1-5km (Figure 4).

Depth (km)	$V_P$ (km/s)	$V_S$ (km/s)	Lithology
0-0.060	1.9	1.28	Weathered Sherwood Sandstone
0.060-0.135	2.75	1.54	Un-weathered Sherwood Sandstone
0.135-0.275	3.1	1.74	Permian
0.275-1.019	3.5	1.97	Coal Measures
1.019-2.751	5.2	2.92	Carboniferous Limestone
2.751-37.751	6.0	3.37	?Precambrian

162

163 Table 1: Seismic velocity structure for New Ollerton area, from *Bishop et al.* (1993).

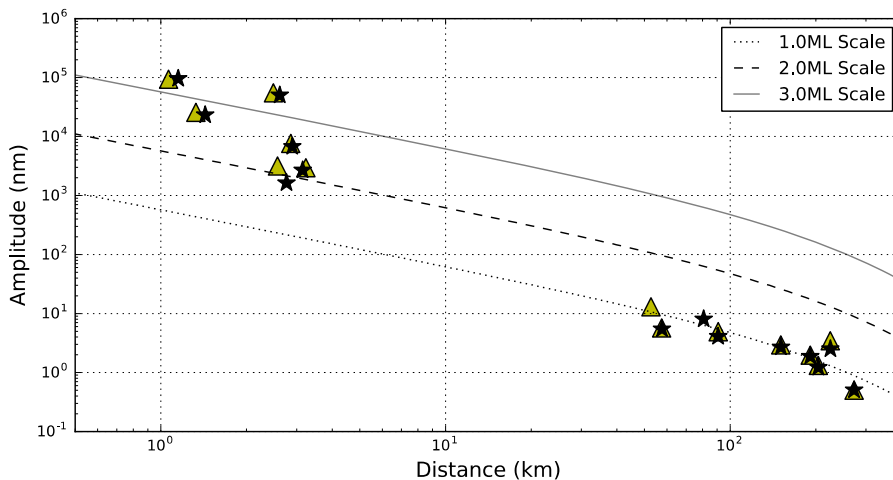
164 Locations of seismic events were determined initially through the inversion of P- and S-wave  
 165 travel time picks, and then relocated with hypoDD (Waldhauser & Ellsworth 2000) using a 1D  
 166 velocity model of Bishop et al. (1993) (Table 1). Local magnitudes were initially calculated using  
 167 displacement measurements made on the NOL network and the existing UK  $M_L$  scale. Of these  
 168 events, those with magnitudes  $> 1.7M_L$  were also in general identifiable on the UK national  
 169 seismic network after the application of a bandpass filter of 3-10Hz. When applying the same  
 170 filtering to the NOL stations, the same discrepancy observed at Preese Hall – an overestimate of  
 171  $M_L$  on nearby stations – is also present in this dataset (Figure 5). This overestimate becomes  
 172 larger as hypocentral distances are reduced.



173

174 Figure 4: Distribution of hypocentral distances and local magnitudes for observations at near New Ollerton.

175 Magnitude are computed using the NOL network and the existing UK local magnitude scale.



176

177 Figure 5: Displacement amplitude versus distance for two events recorded on both the NOL network  
 178 (stations < 5km distance) and the UK national network (stations > 50km distance) for two events  
 179 (2014/02/09 05:33 and 2014/02/12 02:35 coloured yellow and black respectively). Also plotted is the UK  
 180 scale for  $M_L = 1, 2$  and  $3$  (dotted, dashed and solid lines). On the distant stations, the displacements match  
 181 well with the UK scale for an  $M_L = 1.0$  event. On the nearby stations, displacements are substantially larger,  
 182 and this discrepancy increases as hypocentral distance decreases.

#### 183 **4. Velocities and Attenuation**

184 The velocity structure of the UK has been studied by numerous authors (e.g., Chadwick and  
185 Pharaoh 1998; Kelly et al. 2007; Davis et al. 2012), with local P-wave crustal velocity structures  
186 derived from the Lithospheric Seismic Profile in Britain (LISPB) (Kelly et al. 2007) and the  
187 Caledonian Suture Seismic Experiment (Bott et al. 1985). Booth (2010) has also determined  
188 regional 1-D velocity depth models for the northern and central regions of the UK, based on P-  
189 wave arrival from local earthquakes recorded between 1990 and 2008, which compliment the  
190 refraction survey data. Understanding of the S-wave structure comes principally from work in  
191 ambient noise Rayleigh wave tomography (Nicolson et al. 2014) and receiver functions (Davis et  
192 al. 2012; Tomlinson et al. 2006).

193 In general terms the velocity structure in the UK comprises a highly variable sedimentary layer  
194 (Nicolson et al. 2014), overlaying a faster continental basement, on top of a lower crust (Bott et  
195 al. 1985) which extends to the Moho mapped at depths between 25-35km (Chadwick & Pharaoh  
196 1998). Velocities within the sedimentary layer vary significantly depending on composition (see  
197 Table 2); for example, the S-wave velocity of sandstones are typically 1.5km/s, with limestone  
198 higher at approximately 3km/s. Underlying the sedimentary layer, the continental crust is  
199 comprised of crystalline basement rocks, which typically have much higher velocities and can  
200 mark a sharp velocity discontinuity. Abercrombie (1997) has shown that anelastic attenuation,  
201 the inverse of Q, varies substantially between sedimentary and basement rocks. Within the  
202 sedimentary layer Q is typically low (e.g., <30), as demonstrated by Best et al. (2007), while in  
203 the crystalline basement rocks Q increases by at least an order of magnitude (Abercrombie 1995;  
204 Stork & Ito 2004).

205 At New Ollerton the sedimentary layer consists of a combination of sandstones, coal measures,  
206 grit-stones and limestones, which extend to an approximate depth of 2.75km where the  
207 continental basement is encountered (Bishop et al. 1993). The velocity model produced by  
208 Bishop et al. (1993) was derived from borehole information, which extended to the coal

209 measures, and deep seismic refraction data used to constrain the sedimentary-continental crust  
 210 boundary. Best et al. (2007) determined velocities, attenuation and densities of multiple  
 211 sandstone, limestone and siltstone samples collected at depths ranging between 40-185m from  
 212 Whitchester, north-east England using ultrasonic pulse-echo methods. Broadly classifying these  
 213 results by lithology provides the range of velocities, attenuation and densities shown in Table 2,  
 214 which are comparable to the velocities observed at New Ollerton and indicates the likely values  
 215 of Q.

Lithology	$V_P$ (m/s)	$V_S$ (m/s)	$Q_P$	$Q_S$	Density( $kg/m^3$ )
Sandstone	3266±10 – 4807±14	2140±6 – 3076±9	13±1 – 88±32	10±1 – 61±10	2491 – 2620
Limestone	5898±18 – 6301±9	3066±9 – 3275±10	22±1 – 160±88	17±1 – 101±27	2616 – 2661
Siltstone	3372±10 – 4308±13	2024±6 – 2487±7	18±1 – 33±1	10±1 – 26±3	2525 – 2637

216

217 Table 2: P and S wave velocities and Q from laboratory test, from *Best et al.* (2007).

218

## 219 5. Impact of Hypocentral Distance

220 We demonstrate the impact that the sedimentary layer has on the path effects for near-event  
 221 receivers using S-wave apparent velocities and estimates of Q. S-waves are considered as their  
 222 amplitudes that are primarily used to derive  $M_L$ . Because this dataset has limited observation  
 223 within the range 5-20km, events recorded within the general vicinity of New Ollerton are also  
 224 included, which have been sourced from the BGS catalogue.

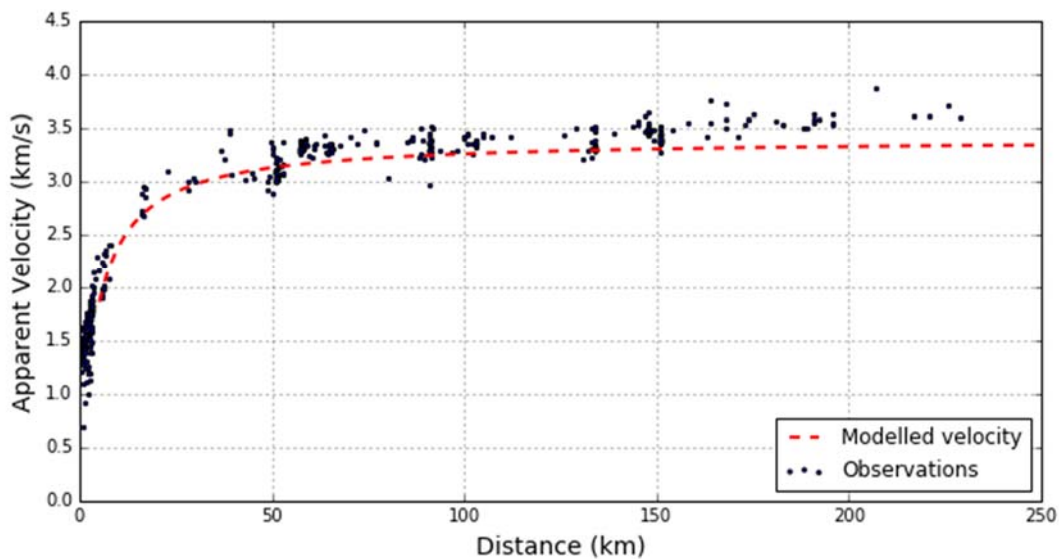
225 In Figure 6 we show the apparent S-wave velocity (the epicentral distance divided by the travel  
 226 time). A prominent “knee” occurs at a distance between 10-15km, with  $V_{app}$  decreasing with  
 227 distance shorter distances, and stabilizing at a value of approximately 3.5km/s at greater  
 228 distances. These observations are modeled using a simple two-layer case, with a shallower layer  
 229 representing sedimentary layers extending to a depth of 4km with a velocity of 2km/s, and a  
 230 deeper layer comprising of the continental basement with a velocity of 3.7km. Travel times ( $TT$ )  
 231 are expressed using □

232 
$$TT = \frac{r}{v_{base}} + \frac{(2z_l - z_s)\cos\theta}{v_{sed}}, \quad (10)$$

233 where  $r$  is the epicentral distance,  $z_l$  is the layer depth,  $z_s$  is the source depth,  $v_{sed}$  and  $v_{base}$  are  
 234 the average sedimentary and crustal layer velocities respectively and  $\theta$  is the take-off angle. The  
 235 modeled apparent velocity ( $V_{app}$ ) is therefore

236 
$$v_{app} = \frac{r}{TT}, \quad (11)$$

237 and it can be seen that the model provides a relatively good fit to the data (Figure 6). This model  
 238 demonstrates that the increase in velocity within the first 10-15km relates to the decreasing  
 239 contribution of the sedimentary layer on the raypath, with signals recorded at distances in excess  
 240 of 10-15km dominated by the faster, less attenuating continental crust.

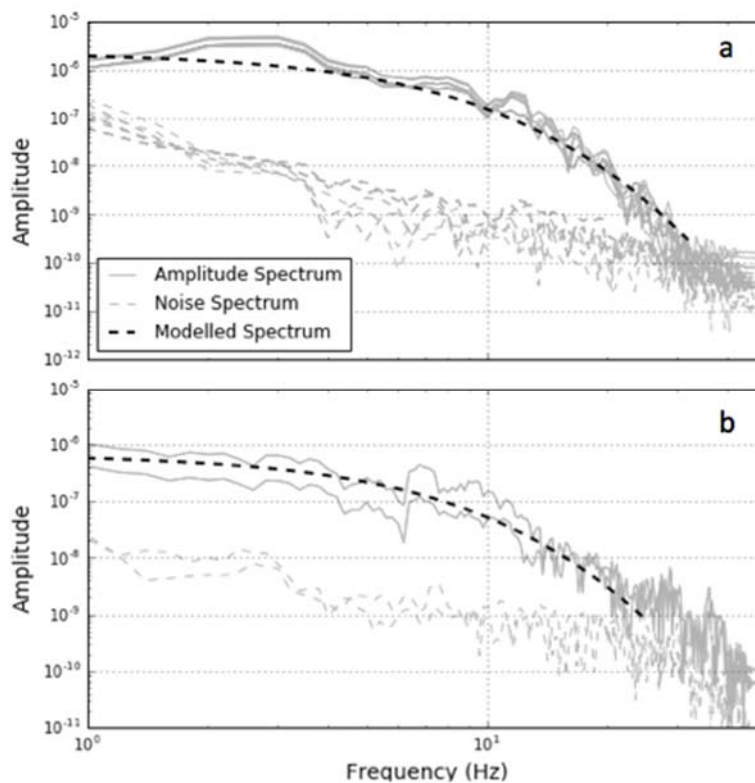


241  
 242 Figure 6: Apparent S-wave velocities from earthquakes within the UK. Red dashed lines represent  
 243 modelled apparent velocities for the simplified 2-layer case, with shallow sedimentary layers of 2.5km/s  
 244 extending to a depth of 2.75km, overlaying a continental basement with a velocity of 3.4km/s.

245 We calculate  $Q$  for eight events recorded on the same station (NOLF), with six 'near' events  
 246 occurring at a distances of approximately 2km and depths of 0.9km and two 'far' events located  
 247 at a distance of 60km and depth of 2.5km. We use spectral methods to estimate the values of  $Q$ ,

248 with displacement spectra generated using the multi-tapering technique developed by Prieto et  
249 al. (2009), and fitted with a Brune model source spectrum (following Prejean & Ellsworth 2001;  
250 Stork et al. 2014). The travel paths of near events have estimated Qs of 30, while the distant  
251 events have estimated Qs of 300.

252 The observations made at small epicentral distances will have significantly different attenuation  
253 effects than the distant observations used by Ottemöller and Sargeant (2013) to calibrate the UK  
254  $M_L$  scale. Ergo a corrected scale must be developed if consistent magnitudes are to be calculated  
255 using stations deployed in close proximity to event epicentres.



256  
257 Figure 7: Source spectra for six 'near' (a) and two 'far' (b) events recorded on station NOLF. The grey  
258 curves show the observed displacement spectra, the grey dashed lines show the noise, and the black  
259 curves show the best-fit Brune model spectra. The 'near' events located at a distances of ~2km and depths  
260 of 0.9km are best-fit by  $Q = 30$ , the 'far' events at an distances of 60km and depths of 2.5km are best-fit  
261 with a  $Q$  of 300.

## 262 6. $M_L$ Scale Recalibration for Nearby Events Based on New Ollerton

263 Many studies have focused on verifying the southern California  $M_L$  scale originally developed by  
 264 Richter (1935), or to recalibrate it for different regions to take into account different attenuation  
 265 properties (e.g. Hutton and Boore 1987; Langston et al. 1998; Keir et al. 2006; Ottemöller and  
 266 Sargeant 2013; Di Bona 2016). The common approach is to invert observations using a least-  
 267 squares method to determine the geometric spreading and attenuation terms, while also solving  
 268 for magnitudes. Recent studies tend to anchor the displacement correction term to 17km, as it is  
 269 easier to adjust the scale to other regions with significantly different attenuation (Alsaker et al.  
 270 1991). Although the events at New Ollerton are in general co-located, and could be considered  
 271 as a single event, we seek to invert the observations in order to gain an indication of the  
 272 appropriate scale required for near-receiver events.

273 We use a Levenberg-Marquardt algorithm, which is a damped least-squares method, to  
 274 determine the best fitting geometrical spreading and attenuation terms at New Ollerton. Due to  
 275 the limited distance range of the observations, attempts to determine these values while also  
 276 treating the magnitudes as an unknown failed to converge. Furthermore, our aim was to create  
 277 a scale that remained consistent with the existing UK local magnitude scale, which has been  
 278 well-established for events recorded on more distant stations. Therefore we instead determined  
 279 the average magnitude discrepancies observed between the NOL network and UK network,  
 280 recalibrate magnitudes and use these values to constrain the inversion. We determined the  
 281 geometric spreading,  $a$ , and attenuation,  $b$ , terms for observed amplitudes,  $A_{ijk}$ , magnitudes,  $M_{Lik}$ ,  
 282 and distances,  $r_{ij}$ , using the model

$$283 \quad \log(A_{ijk}) + 2 = M_{Lik} - a \log\left(\frac{r_{ij}}{17}\right) - b(r_{ij} - 17) \quad (12)$$

284 where index  $i$  labels events, index  $j$  stations, and index  $k$  the component (north-south or east-  
 285 west). Within the data there is evidence of site effects, however we choose to retain simplicity  
 286 through excluding them from the inversion. This approach produces the New Ollerton (NOL)  $M_L$   
 287 scale

288

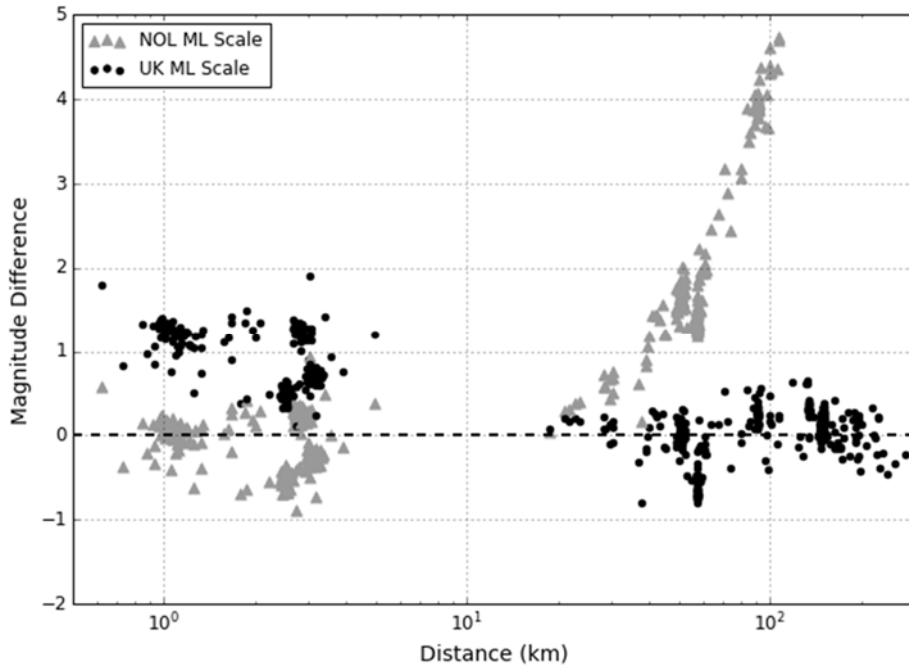
$$M_L = \log(A) + 1.17\log(r) + 0.0514r - 3.0 \quad (13)$$

289 which incorporates the Wood-Anderson gain correction and whose attenuation term, 0.0514, is  
290 an order of magnitude larger than the current UK scale, which is 0.00183.

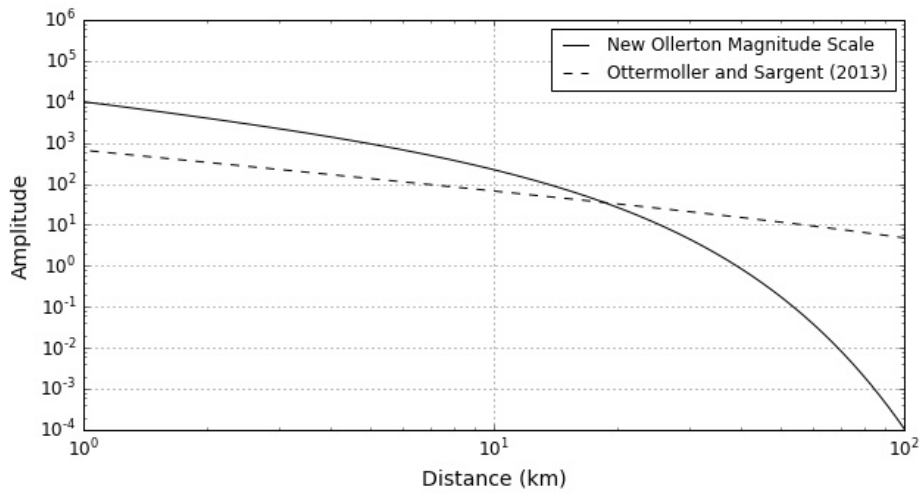
291 We use equation (9) to establish whether the inverted values for  $b$  are reasonable for the two  
292 scenarios (nearby vs distant events). The value for  $b$  calculated by Ottemoller and Sargeant  
293 (2013) of 0.00183 can correspond to an S-wave velocity of 3.5km/s and a Q of 200. The value  
294 for  $b$  calculated here (0.0514) would correspond to an S-wave velocity of 2km/s and a Q of 35.  
295 These are realistic values given the expected raypaths predominantly through the deeper crust,  
296 and through the sediments respectively.

297 Magnitude differences for events observed on both local and regional stations are presented in  
298 Figure 8. We determine the event magnitude through taking the mean  $M_L$  derived from the UK  
299 network and calculated using the UK  $M_L$  scale, then produce differences for all available stations  
300 using the NOL and the UK  $M_L$  scales. The NOL scale successfully removes the discrepancy in  
301 the existing magnitude scale for nearby receivers, and converges with the UK scale at 17km –  
302 the point at which both scales are anchored (Figure 9). There is a lack of data in the range 5-  
303 20km, and after 17km the NOL scale rapidly diverges and introduces large magnitude  
304 discrepancies.





305  
 306 Figure 8: Magnitude differences for New Ollerton events observed on both NOL stations and the UK  
 307 network. The NOL scale corrects the magnitudes at small hypocentral distances, but diverges  
 308 significantly beyond the 17km anchor point.

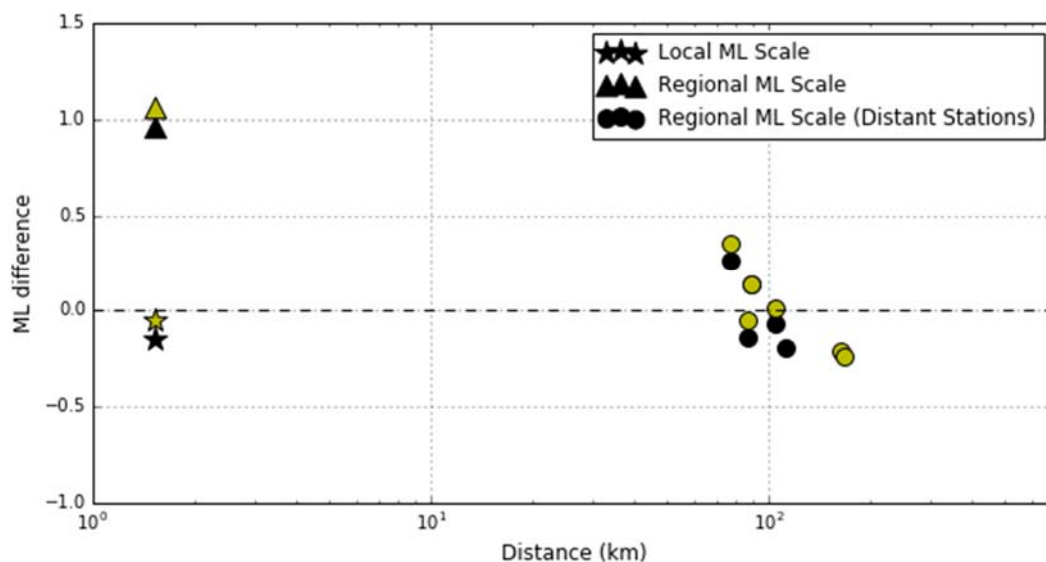


309  
 310 Figure 9: A comparison of the displacements anticipated for an M<sub>L</sub> = 1.0 event, as computed by the  
 311 Ottermoller and Sargeant (2013) scale (dashed line) and that evaluated in equation (13). The scales are  
 312 anchored to a common amplitude at a hypocentral distance of 17km. At smaller distances, the estimated  
 313 ground displacements are different by an order of magnitude.

314 **7. Discussion**

315 While the New Ollerton dataset can be used to understand the impact that near-receiver events  
316 have on  $M_L$  scales, the observations all occur in a single location and over a narrow distance  
317 range. We therefore consider how appropriate the NOL scale is for different UK regions, and the  
318 valid distance range of the scale.

319 Sedimentary layers obviously vary in composition and depth (Kelly et al. 2007; Nicolson et al.  
320 2014), which will influence the attenuation term  $b$ , and the point at which the continental crust  
321 dominates the travel path. We consider the portability of the NOL scale through applying it to two  
322 Preese Hall events observed on both local stations and the UK network (Figure 10). At Preese  
323 Hall the NOL scale has significantly reduced the discrepancy between observed displacements  
324 at the nearby and distant stations (as identified in our introduction), and is now consistent with  
325 the magnitude calculated on the UK network. While in this case the NOL scale appears  
326 appropriate, if the geological composition of the shallow geology is significantly different, for  
327 example limestone dominant, the attenuation term  $b$  may need to be recalibrated.



328  
329 Figure 10: NOL scale (stars) applied to two Preese Hall events observed on the UK network, which  
330 significantly decreases the magnitude difference in contrast to the UK scale (triangles).

331 The depth of the sedimentary-continental interface will influence the cross-over point between

332 the NOL and UK scale. The distance range 5-20km is poorly represented in the New Ollerton  
333 dataset, and over this range that the shift from a travel path dominated by the sedimentary layer  
334 to a path dominated by the continental crust occurs. There are uncertainties in the  
335 appropriateness of using a constant attenuation term over this range which cannot be addressed  
336 by this dataset, as both the apparent velocity and Q will be transitioning from sedimentary layer  
337 to continental crust values.

338 However, most of the UK's shale gas activities expected to take place across the north of  
339 England. Both of the sites considered here (New Ollerton and Preese Hall) fall within the limits  
340 of the Bowland Shale as defined by the BGS. The TLS will usually be administered using  
341 monitoring stations that are within 5km of the proposed wells. We therefore suggest that the  
342 updated magnitude scale developed here is more suitable for the administration of the UK's TLS  
343 than the UK standard  $M_L$  scale.

344

## 345 **7. Conclusions**

346 The UK's hydraulic fracturing TLS will entail the deployment of monitoring stations in close  
347 proximity to well sites. However, the existing UK local magnitude scale is based on observations  
348 of events at significant distances (>50km) from receivers, and so is poorly calibrated for events  
349 recorded on nearby stations (<5km). This discrepancy is significant because for nearby events  
350 the travel path is predominantly within the sedimentary layer, rather than the underlying  
351 basement, and so will require a different attenuation term in the  $M_L$  scale.

352 To address this issue, we studied the earthquakes recorded on a local monitoring network  
353 deployed to monitor coal-mining-induced seismicity at New Ollerton. Through consideration of  
354 apparent velocities, it can be observed that at distances greater than 10-15km the travel paths  
355 of recorded arrivals are predominantly through the continental crust, as S-wave velocities  
356 stabilize at a value of approximately 3.5km/s. However, at closer distances the apparent

357 velocities reduce, implying a greater portion of the raypath is through the overlying sediments. A  
358 significant difference in Q estimates can also be seen between nearby events and distant events,  
359 with lower Q values for nearby events implying greater attenuation through the sedimentary  
360 layers.

361 An updated local magnitude scale has been determined for nearby events using a least-squares  
362 inversion on the New Ollerton data, and we calculate that the attenuation term in the local  
363 magnitude scale should be increased from 0.00183 to 0.0514. This change reflects the slower,  
364 more attenuating nature of sedimentary layer in comparison to the continental crust. A further  
365 indication of the suitability of this scale is provided by the fact that it also removes the ground  
366 motion discrepancies observed for the Preese Hall 2011 events at nearby stations. To ensure  
367 consistent local magnitude estimates during the future operation of the UK's TLS, the updated  
368 magnitude scale should be used when local monitoring networks are within 5km of the event  
369 epicentres.

370

### 371 **Acknowledgements**

372 This work has been funded by the Bristol University Microseismic Projects  
373 ([www1.gly.bris.ac.uk/BUMPS/](http://www1.gly.bris.ac.uk/BUMPS/)), with partial funding also from NERC grant NE/L008351/1. We  
374 thank members of the BUMPS consortium of their technical assistance, particularly Anna Stork.  
375

### 376 **References**

- 377 Abercrombie, R.E., 1995. Earthquake source scaling relationships from -1 to 5 ML using  
378 seismograms recorded at 2.5-km depth. *Journal of Geophysical Research*, 100(B12),  
379 pp.24015–24036.
- 380 Abercrombie, R.E., 1997. Near-surface attenuation and site effects from comparison of surface  
381 and deep borehole recordings. *Bulletin of the Seismological Society of America*, 87(3),  
382 pp.731–744.

383 Alsaker, A. et al., 1991. The ML scale in Norway. *Bulletin of the Seismological Society of*  
384 *America*, 81(2), pp.379–398. Available at:  
385 <http://www.bssaonline.org/content/81/2/379.abstract> N2 - A new local magnitude ML scale  
386 has been developed for Norway, based on a regression analysis of synthesized Wood-  
387 Anderson records. The scale is applicable for distances up to more than 1000 km, and.  
388 Atkinson, G.M. et al., 2014. Estimation of moment magnitude (M) for small events (M<4) on  
389 local networks. , 5(May), pp.1–19.  
390 Best, A.I., Sothcott, J. & McCann, C., 2007. A laboratory study of seismic velocity and  
391 attenuation anisotropy in near-surface sedimentary rocks. *Geophysical Prospecting*,  
392 55(1992), pp.609–625.  
393 Bishop, I., Styles, P. & Allen, M., 1993. Mining-induced seismicity in the Nottinghamshire  
394 Coalfield. *Quarterly Journal of Engineering Geology and Hydrogeology*, 26(4), pp.253–  
395 279. Available at:  
396 <http://qjgeh.lyellcollection.org/cgi/doi/10.1144/GSL.QJEGH.1993.026.004.03>.  
397 Di Bona, M., 2016. A Local Magnitude Scale for Crustal Earthquakes in Italy. *Bulletin of the*  
398 *Seismological Society of America*, 106(1), pp.242–258. Available at:  
399 <http://www.bssaonline.org/lookup/doi/10.1785/0120150155>.  
400 Booth, D.C., 2010. UK 1-D regional velocity models by analysis of variance of P-wave travel  
401 times from local earthquakes. *Journal of Seismology*, 14(2), pp.197–207.  
402 Bott, M.H.P. et al., 1985. Crustal structure south of the lapetus suture beneath northern  
403 England. *Nature*, 314(25), pp.724–727.  
404 Chadwick, R. a. & Pharaoh, T.C., 1998. The seismic reflection Moho beneath the United  
405 Kingdom and adjacent areas. *Tectonophysics*, 299(4), pp.255–279.  
406 Clarke, H. et al., 2014. Felt seismicity associated with shale gas hydraulic fracturing: The first  
407 documented example in Europe. *Geophysical Research Letters*, 41(23), pp.8308–8314.  
408 Available at: <http://doi.wiley.com/10.1002/2014GL062047>.  
409 Davis, M.W. et al., 2012. Crustal structure of the British Isles and its epeirogenic  
410 consequences. *Geophysical Journal International*, 190(2), pp.705–725.

411 Department of Energy and Climate Change, 2015. *Onshore oil and gas exploration in the UK:*  
412 *regulation and best practice,*

413 Eisner, L. et al., 2011. *Seismic analysis of the events in the vicinity of the Preese Hall well,*  
414 Havskov, J. & Ottemoller, L., 2010. *Routine data processing in earthquake seismology: With*  
415 *sample data, exercises and software,* Springer. Available at:  
416 <http://link.springer.com/10.1007/978-90-481-8697-6>.

417 Hutton, L.K. & Boore, D.M., 1987. The MI Scale in Southern California. *Bulletin Of The*  
418 *Seismological Society Of America*, 77(6), pp.2074–2094.

419 IMC Group Consulting Limited, 2003. *Review of the Remaining Reserves at Deep Mines for*  
420 *The Department of Trade and Industry,*

421 Keir, D. et al., 2006. Local earthquake magnitude scale and seismicity rate for the Ethiopian rift.  
422 *Bulletin of the Seismological Society of America*, 96(6), pp.2221–2230.

423 Kelly, A., England, R.W. & Maguire, P.K.H., 2007. A crustal seismic velocity model for the UK,  
424 Ireland and surrounding seas. *Geophysical Journal International*, 171(3), pp.1172–1184.

425 Langston, C. a. et al., 1998. Local magnitude scale and seismicity rate for Tanzania, East  
426 Africa. *Bulletin of the Seismological Society of America*, 88(3), pp.712–721.

427 Nicolson, H., Curtis, A. & Baptie, B., 2014. Rayleigh wave tomography of the British Isles from  
428 ambient seismic noise. *Geophysical Journal International*, 198(2), pp.637–655.

429 O'Toole, T. et al., 2013. Induced seismicity at preese Hall, UK - A review. In *75th European*  
430 *Association of Geoscientists and Engineers Conference and Exhibition 2013 Incorporating*  
431 *SPE EUROPEC 2013: Changing Frontiers.* pp. 5369–5373. Available at:  
432 [https://www.scopus.com/inward/record.uri?eid=2-s2.0-](https://www.scopus.com/inward/record.uri?eid=2-s2.0-84930420017&partnerID=40&md5=333ed7cd90cdb90aa7c8684fcc855da6)  
433 [84930420017&partnerID=40&md5=333ed7cd90cdb90aa7c8684fcc855da6](https://www.scopus.com/inward/record.uri?eid=2-s2.0-84930420017&partnerID=40&md5=333ed7cd90cdb90aa7c8684fcc855da6).

434 Ottemöller, L. & Sargeant, S., 2013. A local magnitude scale ML for the United Kingdom.  
435 *Bulletin of the Seismological Society of ...*, 103(5), pp.2884–2893. Available at:  
436 <http://www.bssaonline.org/cgi/doi/10.1785/0120130085> [Accessed September 17, 2014].

437 Prejean, S.G. & Ellsworth, W.L., 2001. Observation of earthquake source parameters at 2 km  
438 depth in the Long Valley Caldera, Eastern California. *Bulletin of the Seismological Society*

439 *of America*, 91(2), pp.165–177.

440 Prieto, G. a., Parker, R.L. & Vernon, F.L., 2009. A Fortran 90 library for multitaper spectrum  
441 analysis. *Computers and Geosciences*, 35(8), pp.1701–1710.

442 Richter, C.F., 1935. An instrumental earthquake magnitude scale. *Bulletin of the Seismological*  
443 *Society of America*, 25, pp.1–32.

444 Scognamiglio, L. et al., 2012. The 2012 Pianura Padana Emiliana seismic sequence: Locations,  
445 moment tensors and magnitudes. *Annals of Geophysics*, 55(4), pp.549–559.

446 Stork, A.L. & Ito, H., 2004. Source parameter scaling for small earthquakes observed at the  
447 western Nagano 800-m-deep borehole, Central Japan. *Bulletin of the Seismological*  
448 *Society of America*, 94(5), pp.1781–1794.

449 Stork, A.L., Verdon, J.P. & Kendall, J.-M., 2014. The robustness of seismic moment and  
450 magnitudes estimated using spectral analysis. *Geophysical Prospecting*, 62(4), pp.862–  
451 878. Available at: <http://doi.wiley.com/10.1111/1365-2478.12134> [Accessed August 20,  
452 2014].

453 Tomlinson, J.P. et al., 2006. Analysis of the crustal velocity structure of the British Isles using  
454 teleseismic receiver functions. *Geophysical Journal International*, 167(1), pp.223–237.

455 Waldhauser, F. & Ellsworth, W.L., 2000. A Double-difference Earthquake location algorithm:  
456 Method and application to the Northern Hayward Fault, California. *Bulletin of the*  
457 *Seismological Society of America*, 90(6), pp.1353–1368.

458 Westaway, R., 2016. The importance of characterizing uncertainty in controversial geoscience  
459 applications: induced seismicity associated with hydraulic fracturing for shale gas in  
460 northwest England. *Proceedings of the Geologists' Association*, 127(1), pp.1–17. Available  
461 at: <http://eprints.gla.ac.uk/119683/>.

462 Wilson, M.P. et al., 2015. Anthropogenic earthquakes in the UK: A national baseline prior to  
463 shale exploitation. *Marine and Petroleum Geology*, 68, pp.1–17. Available at:  
464 <http://dx.doi.org/10.1016/j.marpetgeo.2015.08.023>.

465